


Ultrafast transient absorption spectroscopy of strongly correlated Mott insulators

Youngjae Kim ^{*}*School of Physics, KIAS, Seoul 02455, Korea*

(Received 19 March 2023; revised 22 June 2023; accepted 26 June 2023; published 12 July 2023)

We applied time-resolved transient absorption spectroscopy to systematically investigate the ultrafast optical responses of condensed matter systems. Under an intense pump pulse, absorption spectra indicate that the noninteracting electrons of band insulators produce a field-induced redshift, known as the dynamical Franz-Keldysh effect, as commonly expected. In contrast to band insulators, in Mott insulators, unconventional spectra are observed which do not fully reflect the dynamical Franz-Keldysh effect. While the spectra still exhibit fishbonelike structures mimicking the dynamical Franz-Keldysh effect, they show a negative difference absorption below the band edge, rendering a blueshift. In addition, the decomposed calculation reveals that the negative difference absorption is mainly contributed from the creation and the annihilation of transient double occupancy, implying that the unconventional spectra are purely driven by the electron correlations. These demonstrated unconventional responses can guide us to better understanding of the correlation-originated ultrafast electron dynamics in condensed matter systems.

DOI: [10.1103/PhysRevB.108.035122](https://doi.org/10.1103/PhysRevB.108.035122)

I. INTRODUCTION

As ultrashort laser technologies have been developed in recent decades they have achieved attosecond (as) temporal resolution ($1 \text{ as} = 10^{-18} \text{ s}$), which allows access to new insights into the $10 - 100 \text{ as}$ time domain, which is shorter than the typical time scale of electron dynamics [1–4]. This has led to the development of attosecond transient absorption spectroscopy (TAS), which is capable of naturally capturing the electron dynamics in matter. TAS has become an essential technique for investigating highly nonlinear responses and their transient spectral properties at extreme time scales within subcycle laser pulses [5–7]. In its early stage, attosecond TAS was widely used to demonstrate the dynamics of atomistic systems [6–9], and more recently it has been extended to condensed matter systems, to explore crystal symmetries [10], electronic structure renormalization [11], dipole responses [12], measuring photocarriers [13,14], and the dynamical Franz-Keldysh effect (DFKE) [15–21].

Among these studies, one of the essential achievements has been the control of fundamental properties using an electric field to directly establish electronic responses. When condensed matter is exposed to an intense external electric field, the resulting absorption spectra are modified because of field-induced additional channels, leading to a redshift below the band edge, referred to as the Franz-Keldysh effect (FKE) [22–25].

Recent studies have reported a temporally extended scheme of the FKE under an alternating electric field, known as the DFKE, with pump-induced intraband transitions to reveal intriguing features of real time phase oscillations, like fishbone structures, in addition to the redshift of the FKE

[10,21]. It also has been observed that the dynamical nature of the DFKE can be characterized in the crossover regime of the adiabatic parameter $\gamma_a (= U_{\text{pon}}/\omega_p) \sim 1$, the intermediate regime between the pump photon energy ω_p and the ponderomotive energy U_{pon} . Then the FKE begins to appear in the adiabatic regime, i.e., $\gamma_a \gg 1$ [17,18,26]. Several studies on the DFKE in condensed matter systems have been reported from experiments on a diamond, where the absorption modified by the intense pump pulse was directly captured by probe (XUV) [20]. The results were also supported by a theoretical approach, time-dependent density functional theory (TDDFT), to show the oscillating property of absorption as well as the phase delay.

More recently, nontrivial phenomena found in the attosecond transient reflectivity have been deeply resolved to incorporate excitonic dynamics of atomistic attribute in condensed matter systems [4]. This implies that the combined nature could provide unexpected insights into ultrafast dynamics. In addition, a study of the ultrafast TAS of multiband charge transfer insulators within the framework of TDDFT + U (with a dynamical modification of the Hubbard U) has pointed out that the screening of U would affect and change spectra of TAS beyond the DFKE [27]. However, the response of ultrafast TAS for a pure Mott phase still remains unclear. Considering the preceding results, it would be timely to suggest an exquisite signature from the TAS to determine whether the dynamics of condensed matter systems are purely associated with their rather strong electron correlation.

In this study, by employing the real-time exact diagonalization method, we shall demonstrate the ultrafast TAS to explore the unbiased results of dynamics from band insulators and Mott insulators. In band insulators, an intense pump pulse induces a modification in absorption corresponding to the DFKE, which trivially accompanies the redshift, i.e., increased absorption, below the band edge and the

^{*}Corresponding author: ykim.email@gmail.com

V-shaped phase oscillations like fishbone structures that result from the intraband motion of electrons. However, in contrast to the DFKE, in Mott insulators, where the insulating band structures purely originate from the electron correlation, the ultrafast TAS reveals an unconventional modification in their spectra, which appears to show a blueshift below the band edge, violating the DFKE, while the fishbonelike structures still exist, mimicking the DFKE. Furthermore, by investigating the decomposed difference spectra of the TAS from the Mott insulators, we determined that the transition pathways associated with the creation and annihilation of transient double occupancy, a special state due to on-site repulsions, evidently contributes to the blueshift. Understanding the unconventional signals from the ultrafast TAS for the Mott insulator can provide insight into the dynamical linking between the electron correlation and the ultrafast responses, which can guide us to the correlation-originated ultrafast dynamics in condensed matter systems.

II. ULTRAFAST TAS OF BAND INSULATORS AND MOTT INSULATORS

We write model Hamiltonians [28] to describe one-dimensional periodic solids with a finite size $L = 8$, which reads

$$\mathcal{H}_B = -t_h \sum_{i,\sigma} (c_{i,\sigma}^\dagger c_{i+1,\sigma} + \text{H.c.}) + \Delta/2 \sum_{i,\sigma} (-1)^i n_{i,\sigma} \quad (1)$$

for band insulators where the fully noninteracting electrons are considered, and Δ corresponds to the staggered crystal potential for ionic materials. And,

$$\mathcal{H}_M = -t_h \sum_{i,\sigma} (c_{i,\sigma}^\dagger c_{i+1,\sigma} + \text{H.c.}) + U \sum_i n_{i,\uparrow} n_{i,\downarrow} \quad (2)$$

for Mott insulators where the electrons are strongly correlated via the Hubbard U for on-site repulsion. The $c_{i\sigma}^\dagger$ ($c_{i\sigma}$) is the creation (annihilation) operator for an electron with spin $\sigma : \uparrow, \downarrow$ at site i , the hopping t_h , and the number operator $n_{i,\sigma} = c_{i,\sigma}^\dagger c_{i,\sigma}$.

After the half-filled ground state $|\Psi(\tau \rightarrow -\infty)\rangle = |\Psi_0\rangle$ is obtained, we perform the time-dependent calculation under a given light wave by solving the time-dependent Schrödinger equation $i\partial/\partial\tau|\Psi(\tau)\rangle = \mathcal{H}_{B(M)}(\tau)|\Psi(\tau)\rangle$, within the fourth-order Runge-Kutta algorithm [29]. The time-dependent Hamiltonian is evolved from the Peierls phase [30] $t_h \rightarrow t_h(\tau) = t_h e^{-i(e/\hbar)A(\tau)d_l/c}$, with the vector potential $A(\tau)$, the speed of light c , the elementary charge e , the Planck constant \hbar , and the distance between nearest-neighbor sites d_l . Hereafter, we consider a set of atomic unit (a.u.) systems, in which $e = \hbar = 1$ a.u., and we simply set the $d_l = 1$ a.u. To evaluate the optical conductivity, we carry out a real time current [30,31] $J(\tau) = \langle \Psi(\tau) | j(\tau) | \Psi(\tau) \rangle$ with a current operator $j(\tau) = -c\partial/\partial A(\tau)\mathcal{H}_{B(M)}(\tau)$. Then, one can obtain the real part of the conductivity as

$$\sigma_1(\omega) = \text{Re}[J(\omega)/E(\omega)] \quad (3)$$

from the current $J(\omega) = \int d\tau e^{-\eta\tau + i\omega\tau} J(\tau)$ and electric field $E(\omega) = \int d\tau e^{-\eta\tau + i\omega\tau} E(\tau)$, with the relation of $E(\tau) = -(1/c)\partial/\partial A(\tau)$ and the smear parameter $\eta/t_h = 0.4$. The probe is defined as $A(\tau) \rightarrow A_{pr}(\tau) = A_{pr0}\phi(\tau)$ with

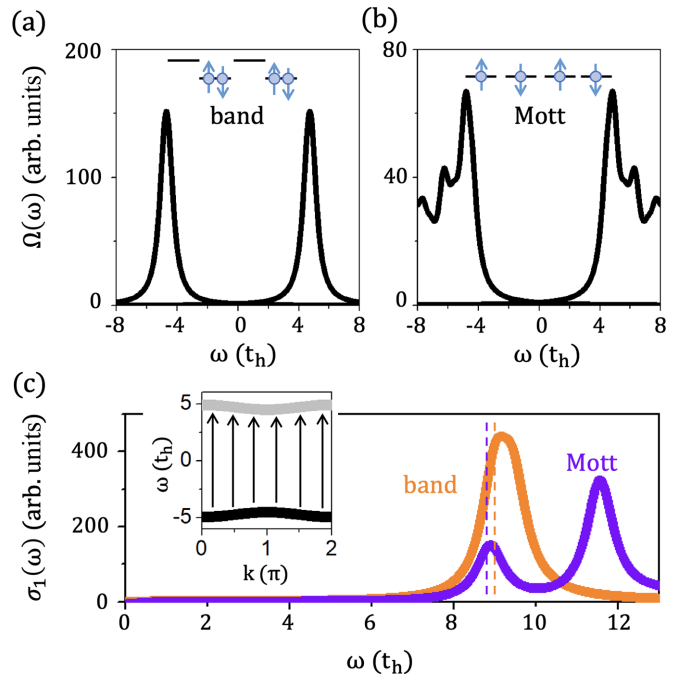


FIG. 1. Calculated spectral weights and optical conductivity. (a), (b) Spectral weights of band insulators (a) and Mott insulators (b). The schematics in (a), (b) denote the ground electronic configurations and site energies. (c) The optical conductivity of ground states $\sigma_1(\omega)$ of the band insulators and the Mott insulators. We fix the parameters of the staggered potential $\Delta/t_h = 9$ for (a) and the Hubbard potential $U/t_h = 12$ for (b), respectively, hereafter. The inset in (c) depicts the probe-induced absorption process from the valence to the conduction bands. The dashed lines indicate the frequencies of each band edge.

$A_{pr0} = 0.001t_h$ and $\phi(\tau)$ the Heaviside step function, thus $E(\tau) = E_{pr}\delta(\tau)$ with small E_{pr} to guarantee a linear response.

In Fig. 1, we display the ground state properties of the band insulator and the Mott insulator. Under given parameters Δ and U , the energy scales represented by the spectral weights have similar insulating phases, as seen from the Figs. 1(a) and 1(b). The spectral weights are extracted by the Lehmann representation [32] $\Omega(\omega) = \text{Im}[(1/\pi) \sum_{i,\sigma} [\langle \Psi_0 | c_{i,\sigma}^\dagger 1/(\omega + E_0 - \mathcal{H}_{B(M)} + i\eta) c_{i,\sigma} | \Psi_0 \rangle - \langle \Psi_0 | c_{i,\sigma} 1/(\omega + E_0 - \mathcal{H}_{B(M)} + i\eta) c_{i,\sigma}^\dagger | \Psi_0 \rangle]$, and the E_0 denotes the ground state eigenvalue corresponding to the ground eigenstate $|\Psi_0\rangle$. Strong correlations in the Mott insulator lead to slightly wider bandwidths than that of the band insulator. In Fig. 1(c), the conductivity is found to have the lowest transitions at similar band edge frequencies of $\omega/t_h = 9$ for the band insulator and $\omega/t_h = 8.8$ for the Mott insulator, respectively. Hence the energy scales for the TAS of both systems would be similar to each other.

Next, we applied the TAS to explore a real-time modification in the transient spectra, as shown in Fig. 2. In the calculation, the vector potential contains both the pump and probe fields [10], i.e., $A(\tau) = A_p(\tau) + A_{pr}(\tau - \tau_d)$ with a pump-probe time delay τ_d . The first term describes the single packet of the pump pulse as $A_p(\tau) = A_{p0} \sin(\omega_p\tau) \cos^2(0.5\pi\tau/d)$ for $|\tau| \leq d$ and $A_p(\tau) = 0$ for otherwise. The pump length parameter for an ultrashort pulse

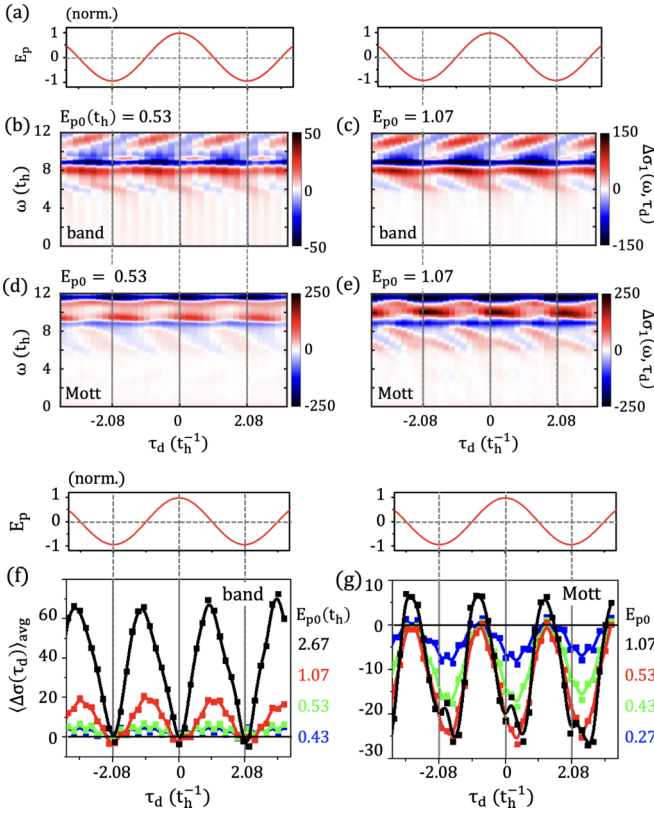


FIG. 2. Calculated difference spectra of the pump-probe spectroscopy; the TAS and the averaged TAS for the band insulator and the Mott insulator. (a) Time profile of the normalized electric field of the pump pulse with frequency of $\omega_p/t_h = 1.5$, and $\omega_p \ll \Delta$ and $\omega_p \ll U$, i.e., off-resonance excitation. (b)–(e) $\Delta\sigma_1$ as a function of τ_d of the band insulator (b), (c) and the Mott insulator (d), (e) under different peak electric field strengths E_{p0} of $E_{p0} = A_{p0}\omega_p/c$. (f),(g) The averaged TAS below the band edge $\langle\Delta\sigma(\tau_d)\rangle_{\text{avg}}$ for the band insulator (f) and the Mott insulator (g). The calculation of the averaged TAS is performed by $\langle\Delta\sigma(\tau_d)\rangle_{\text{avg}} = 1/\epsilon \int_{\epsilon_E - \epsilon}^{\epsilon_E} d\omega \Delta\sigma_1(\omega, \tau_d)$ at every given τ_d . The range of the average is $\epsilon/t_h = 2$, and the band edge is $\epsilon_E/t_h = 9$ for the band insulator (f) and the $\epsilon_E/t_h = 8.8$ for the Mott insulator (g).

is fixed as $d = 9\pi/\omega_p$ to include 9 periods of optical cycles in a single packet. The transient current becomes $J_{ir}(\tau, \tau_d) = J_{p+pr}(\tau, \tau_d) - J_p(\tau)$. The $J_{p+pr}(\tau, \tau_d)$ should be the current when the $\mathcal{H}_{B(M)}(\tau)$ is evolved by the vector potential $A(\tau) = A_p(\tau) + A_{pr}(\tau - \tau_d)$ and similarly, $J_p(\tau)$ under $\mathcal{H}_{B(M)}(\tau)$ of the $A(\tau) = A_p(\tau)$. Finally, the difference spectra of TAS, which we shall call just TAS hereafter, is practically obtained as [10]

$$\Delta\sigma_1(\omega, \tau_d) = \text{Re}[J_{ir}(\omega, \tau_d)/E_{pr}(\omega, \tau_d)] - \sigma_1(\omega), \quad (4)$$

and the probe electric field is $E_{pr}(\tau, \tau_d) = -(1/c)\partial/\partial\tau A_{pr}(\tau - \tau_d)$. In Fig. 2(a), the time profile of the pump electric field is shown with a relation $E_p(\tau_d) = -(1/c)\partial/\partial\tau A_p(\tau)|_{\tau=\tau_d}$. In Figs. 2(b) and 2(c), the TAS from the band insulator exhibits three properties: (i) the redshift of absorption below the band edge, (ii) the fishbone structures [33], and (iii) increased transparency at the band edge [34]. These results typically represent the

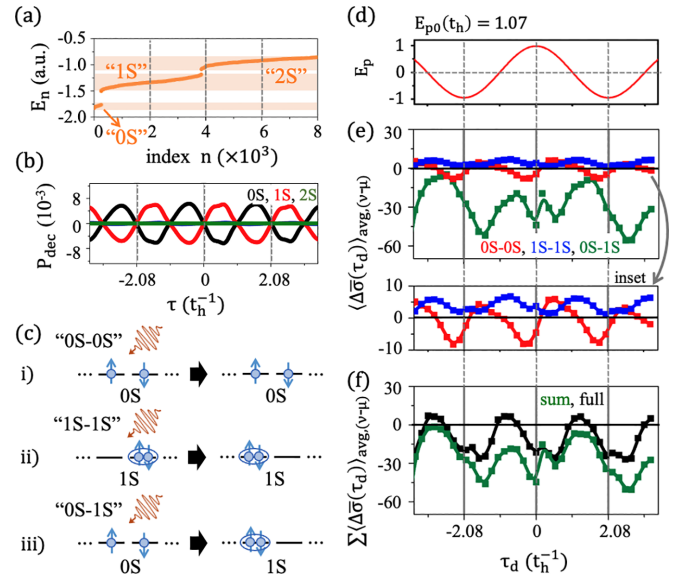


FIG. 3. Decomposed calculation of TAS for the Mott insulator with $E_{p0}(t_h) = 1.07$. (a) Eigenvalues E_n corresponding to each index number n of the Mott insulator. (b) The transition rate between the decomposed set of eigenstates. (c) Schematics of the main transition pathways for the decomposed TAS, i.e., 0S-0S, 1S-1S, and 0S-1S. (d) The time profile of the pump pulse. (e) The averaged decomposed TAS $\langle\Delta\sigma(\tau_d)\rangle_{\text{avg},(v-\mu)}$ of $v-\mu$ for 0S-0S, 1S-1S, and 0S-1S. The inset is the zoomed results of the 0S-0S, 1S-1S. (f) The summation of the averaged decomposed TAS $\sum_{(v-\mu)} \langle\Delta\sigma(\tau_d)\rangle_{\text{avg},(v-\mu)}$, including components of 0S-0S, 1S-1S, and 0S-1S. Note, the full calculation is from Fig. 2(g).

fingerprint of the DFKE [10,18,21]. In Figs. 2(d) and 2(e), for the Mott insulator however, a distinctively nontrivial TAS result is captured, in comparison to the band insulator. It is interesting to note that while the fishbonelike structure still appears, mimicking the DFKE, a blueshift bearing a negative difference absorption below the band edge is observed. In addition, the responses of the phase oscillations are robust, regardless of the field strength of the pump pulse. These findings clearly show the transient dynamics of virtually excited carriers (see Fig. 1, Ref. [35]).

In order to more deeply understand the dynamics recorded by the TAS from the Mott insulator, as compared with the band insulator, we show the averaged TAS below the band edge in Figs. 2(f) and 2(g). In both systems, the results of the averaged TAS commonly exhibit the $2\omega_p$ oscillations of its phases. Furthermore, the phase delays between the TAS and the pump electric field are found to be out-of-phase, meaning the current responses are primarily governed by the dynamical nature [18] (see Figs. 2 and 3, Ref. [35]).

On the other hand, in the results, the sign of the spectra clearly distinguish the band insulator and the Mott insulator. The averaged TAS from the band insulator completely shows a positive sign, corresponding to the DFKE, since there are allowed probe channels assisted by the pump, as shown in Fig. 2(f). In contrast, in the Mott insulator in Fig. 2(g), it is remarkable that the averaged TAS has a mostly negative sign, which does not obey the DFKE. Therefore, we emphasize that the unconventional TAS result observed in the Mott insulator is nontrivial, and this consequently makes it necessary

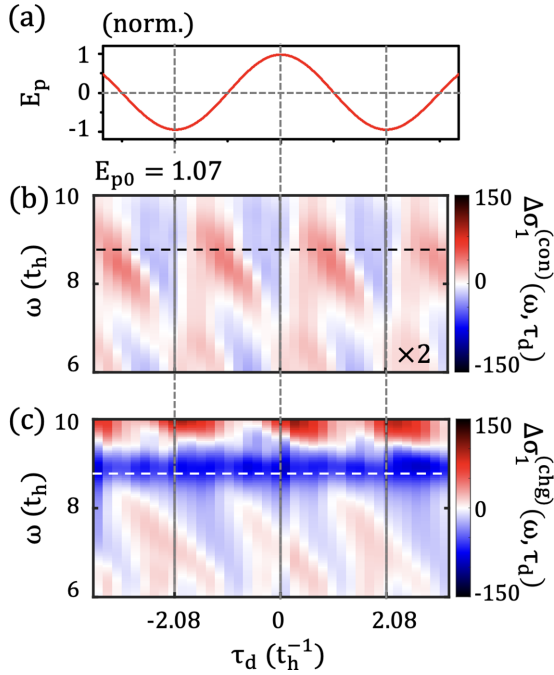


FIG. 4. Decomposed TAS of the Mott insulator in the ω - τ_d with $E_{p0}(t_h) = 1.07$. (a) Time profile of the electric field of pump pulse. (b) Decomposed TAS containing the transitions of number-conserved double occupancies $\Delta\sigma_1^{(\text{con})}(\omega, \tau_d) = \Delta\bar{\sigma}_1(\omega, \tau_d)_{(0S-0S)} + \Delta\bar{\sigma}_1(\omega, \tau_d)_{(1S-1S)}$. (c) Decomposed TAS containing the transitions of number-changed double occupancies $\Delta\sigma_1^{(\text{chg})}(\omega, \tau_d) = \Delta\bar{\sigma}_1(\omega, \tau_d)_{(0S-1S)}$.

to establish the underlying physics when the pure electron correlation is incorporated into the TAS.

When the electric field strength is more strongly enhanced, the phase delay of the band insulator gradually decreases and becomes in-phase, as featured in the adiabatic regime $\gamma_a (= U_{\text{pon}}/\omega_p) \gg 1$ (see the details on γ_a in Fig. 3, Ref. [35]) with $U_{\text{pon}} = A_{p0}^2/4\mu c^2$ where A_{p0} , μ , and ω_p represent the amplitude of the vector potential of the pump pulse, the reduced mass of the band insulator, and the frequency of the pump pulse, respectively [18]. In the Mott insulator, however, the phase delay in this regime ($\gamma_a \gg 1$) cannot be simply defined. Since structureless signals are introduced by the strong electron correlations, the adiabatic responses of the FKE could not be monitored in the Mott insulator (see Figs. 3 and 4, Ref. [35]).

III. DYNAMICS OF DOUBLE OCCUPANCY

As seen from Fig. 2, the important feature separating the band insulator and the Mott insulator is the sign of the TAS below the band edge. Thus we establish the relevant dynamical links between the sign of the TAS and the electron correlation. We apply the decomposed calculation of the TAS for the Mott insulator shown in Fig. 3. In Fig. 3(a), the eigenvalues of the n th index E_n , with corresponding eigenstates following the $\mathcal{H}_M|\Psi_n\rangle = E_n|\Psi_n\rangle$, are depicted. As the index n increases, the eigenvalue also continuously increases. As reported in a previous study [29], one can see some discontinuous points dividing the groups of eigenstates with respect to the number of double occupancies. Therefore, the 0S, 1S,

2S, and so on correspond to groups containing eigenstates with a given number of double occupancies: 0, 1, 2, and so on, respectively. To investigate the main transition pathways related to the number of double occupancies, we compute the transition rate between decomposed eigenstates, $P_{\text{dec}}(\tau) = \partial/\partial\tau \sum_{n\in\nu} |\langle\Psi_n|\Psi(\tau)\rangle|^2$ with ν indicating each group, i.e., 0S, 1S, and 2S, as shown in Fig. 3(b). From the results, the significant transition pathways are observed to mostly include 0S and 1S. The pathways containing 2S and higher terms should rarely be important in the present dynamics. Therefore, we will mainly focus on the transition pathways made of 0S and 1S as displayed in Fig. 3(c). The transition between the 0S and 1S should be accompanied by a change in the number of double occupancies, while the others conserve their numbers. One can consequently decompose the TAS into two transition groups: First, the transitions comprising the number-conserved double occupancies (0S-0S and 1S-1S), and second, transitions comprising the number-changed double occupancies (0S-1S), respectively.

From the above discussion, one can define the decomposed TAS by following the new current operator $\vec{j}(\tau)_{(v-\mu)}$ on the basis of $j(\tau)_{v,\mu}$, we have

$$j(\tau) \rightarrow j(\tau)_{v,\mu} = \sum_{n\in\nu, m\in\mu} |\Psi_n\rangle\langle\Psi_n|j(\tau)|\Psi_m\rangle\langle\Psi_m|, \quad (5)$$

with ν and μ belonging to the groups 0S and 1S; that is, the transitions of the number-conserved double occupancies will be $\vec{j}(\tau)_{(0S-0S)} = j(\tau)_{0S,0S}$ and $\vec{j}(\tau)_{(1S-1S)} = j(\tau)_{1S,1S}$, and the number-changed double occupancies $\vec{j}(\tau)_{(0S-1S)} = j(\tau)_{1S,0S} + j(\tau)_{0S,1S}$. After calculating $\vec{j}(\tau)_{(v-\mu)}$, the previous Eqs. (3) and (4) can be rewritten to be the decomposed TAS as follows: $\sigma_1(\omega) \rightarrow \bar{\sigma}_1(\omega)_{(v-\mu)}$ and $\Delta\sigma_1(\omega, \tau_d) \rightarrow \Delta\bar{\sigma}_1(\omega, \tau_d)_{(v-\mu)}$, respectively, and eventually the averaged decomposed TAS $\langle\Delta\bar{\sigma}(\tau_d)\rangle_{\text{avg},(v-\mu)}$ can be computed. Note, $\langle\Delta\bar{\sigma}(\tau_d)\rangle_{\text{avg},(v-\mu)} = 1/\epsilon \int_{\epsilon_E-\epsilon}^{\epsilon_E} d\omega \Delta\bar{\sigma}_1(\omega, \tau_d)_{(v-\mu)}$ with the same parameters ϵ and ϵ_E used in the caption of Fig. 2. In Fig. 3(e), we represent the $\langle\Delta\bar{\sigma}(\tau_d)\rangle_{\text{avg},(v-\mu)}$ of $v-\mu$ for 0S-0S, 1S-1S, and 0S-1S. It is worth noting that the TAS obtained from the 0S-0S and 1S-1S are found to show partially positive and fully positive signs. In contrast, the transitions for 0S-1S become special pathways since the strong electron correlation brings about a change in the many-body energies $\sim U$ equivalent to forming a double occupancy. It is discovered that the difference spectra of 0S-1S dominantly carry a negative sign, which entirely reproduces the full calculation [see Figs. 3(e) and 3(f)]. As a result, we note that these pathways including 0S-1S mainly give rise to a negative sign, which is the signature of the creation and the annihilation of transient double occupancy, and clearly measured by TAS.

Finally, to support our claims, we plot the decomposed TAS with the ω - τ_d analysis as depicted in Fig. 4. In Fig. 4(b), the TAS of transitions including the number-conserved double occupancies $\Delta\sigma_1^{(\text{con})}$ are found to have positive signals below the band edge and out-of-phase, which partially represents a feature of the DFKE as given in Figs. 2(b) and 2(c). In Fig. 4(c), however, the TAS of the number-changed double occupancies $\Delta\sigma_1^{(\text{chg})}$ exhibits highly negative signals below the band edge, which quantitatively overwhelms the $\Delta\sigma_1^{(\text{con})}$ due to the nontrivial excitations for strong electron correlations [36,37] (see Fig. 5, Ref. [35]). In addition, the silhouette

in Fig. 4(c) also qualitatively reproduces the results of the full calculation. Although the exact diagonalization in our current study is applicable to a finite periodic size, the dynamics of double occupancy would be robust even in larger sizes [38].

Our primary focus in this study is on the ultrafast TAS of pure Mott insulators within the $\gamma_a \sim 1$ regime, corresponding to the DFKE. The transient dynamics of double occupancy, as based on the Hubbard model in Eq. (2), reveals strikingly different responses compared to those predicted in the DFKE. However, when paired as doublon-holon with nearest-neighbor Coulomb repulsion within the extended Hubbard model for organic salts, double occupancy would offer promising features [39,40]. Therefore, a deeper understanding of the interactions within a wider range of correlated electron systems remains an intriguing area of study for ultrafast TAS.

In summary, we report ultrafast TAS from band insulators and Mott insulators. In the band insulators, as commonly expected, trivial responses are found to accompany the redshift below the band edge and the fishbone structures. In the Mott

insulator, however, where the system is associated with pure electron correlation, unconventional TAS results are observed with a blueshift below the band edge, which violates the DFKE, but the fishbonelike structures still exist. It is also found that the transitions for the creation and the annihilation of transient double occupancy evidently contribute to the unconventional difference spectra leading to the blueshift. Our study to establish the unconventional ultrafast TAS results, incorporating pure electron correlation, provides a novel insight into the correlation-originated ultrafast electron dynamics in condensed matter.

ACKNOWLEDGMENTS

We are grateful to J. D. Lee for the fruitful discussion. The authors thank the computational support from the Center for Advanced Computation (CAC) at Korea Institute for Advanced Study (KIAS). In this study, Y.K. supported by a KIAS Individual Grant (Grant No. PG088601) at Korea Institute for Advanced Study (KIAS).

-
- [1] R. Kienberger, E. Goulielmakis, M. Uiberacker, A. Baltuska, V. Yakovlev, F. Bammer, A. Scrinzi, Th. Westerwalbesloh, U. Kleineberg, U. Heinzmann, M. Drescher, and F. Krausz, *Nature (London)* **427**, 817 (2004).
- [2] A. L. Cavalieri, N. Müller, Th. Uphues, V. S. Yakovlev, A. Baltuška, B. Horvath, B. Schmidt, L. Blümel, R. Holzwarth, S. Hendel, M. Drescher, U. Kleineberg, P. M. Echenique, R. Kienberger, F. Krausz, and U. Heinzmann, *Nature (London)* **449**, 1029 (2007).
- [3] F. Krausz and M. Ivanov, *Rev. Mod. Phys.* **81**, 163 (2009).
- [4] M. Lucchini, S. A. Sato, G. D. Lucarelli, B. Moio, G. Inzani, R. Borrego-Varillas, F. Frassetto, L. Poletto, H. Hübener, U. D. Giovannini, A. Rubio, and M. Nisoli, *Nat. Commun.* **12**, 1021 (2021).
- [5] M. Holler, F. Schapper, L. Gallmann, and U. Keller, *Phys. Rev. Lett.* **106**, 123601 (2011).
- [6] H. Wang, M. Chini, S. Chen, C. H. Zhang, F. He, Y. Cheng, Y. Wu, U. Thumm, and Z. Chang, *Phys. Rev. Lett.* **105**, 143002 (2010).
- [7] E. Goulielmakis, Z.-H. Loh, A. Wirth, R. Santra, N. Rohringer, V. S. Yakovlev, S. Zherebtsov, T. Pfeifer, A. M. Azzeer, M. F. Kling, S. R. Leone, and F. Krausz, *Nature (London)* **466**, 739 (2010).
- [8] M. Chini, B. Zhao, H. Wang, Y. Cheng, S. X. Hu, and Z. Chang, *Phys. Rev. Lett.* **109**, 073601 (2012).
- [9] L. Drescher, M. J. J. Vrakking, and J. Mikosch, *J. Phys. B: At. Mol. Opt. Phys.* **53**, 164005 (2020).
- [10] S. A. Sato, H. Hübener, U. D. Giovannini, and A. Rubio, *Appl. Sci.* **8**, 1777 (2018).
- [11] M. Schultze, K. Ramasesha, C. D. Pemmaraju, S. A. Sato, D. Whitmore, A. Gandman, J. S. Prell, L. J. Borja, D. Prendergast, K. Yabana, D. M. Neumark, and S. R. Leone, *Science* **346**, 1348 (2014).
- [12] H. Mashiko, K. Oguri, T. Yamaguchi, and A. Suda, and H. Gotoh, *Nat. Phys.* **12**, 741 (2016).
- [13] F. Schlaepfer, M. Lucchini, S. A. Sato, M. Volkov, L. Kasmi, N. Hartmann, A. Rubio, L. Gallmann, and U. Keller, *Nat. Phys.* **14**, 560 (2018).
- [14] M. Zürch, H.-T. Chang, L. J. Borja, P. M. Kraus, S. K. Cushing, A. Gandman, C. J. Kaplan, M. H. Oh, J. S. Prell, D. Prendergast, C. D. Pemmaraju, D. M. Neumark, and S. R. Leone, *Nat. Commun.* **8**, 15734 (2017).
- [15] Y. Yacoby, *Phys. Rev.* **169**, 610 (1968).
- [16] A. P. Jauho and K. Johnsen, *Phys. Rev. Lett.* **76**, 4576 (1996).
- [17] F. Novelli, D. Fausti, F. Giusti, F. Parmigiani, and M. Hoffmann, *Sci. Rep.* **3**, 1227 (2013).
- [18] T. Otoe, Y. Shinohara, S. A. Sato, and K. Yabana, *Phys. Rev. B* **93**, 045124 (2016).
- [19] M. Du, C. Liu, Y. Zheng, Z. Zeng, and R. Li, *Phys. Rev. A* **100**, 043840 (2019).
- [20] M. Lucchini, S. A. Sato, A. Ludwig, J. Herrmann, M. Volkov, L. Kasmi, Y. Shinohara, K. Yabana, L. Gallmann, and U. Keller, *Science* **353**, 916 (2016).
- [21] M. Lucchini, S. A. Sato, F. Schlaepfer, K. Yabana, L. Gallmann, A. Rubio, and U. Keller, *J. Phys.: Photon.* **2**, 025001 (2020).
- [22] W. Franz, *Z. Naturforschung* **13**, 484 (1958).
- [23] L. V. Keldysh, *J. Exptl. Theoret. Phys. (USSR)* **33**, 994 (1957) [*Sov. Phys. JETP* **6**, 673 (1958)].
- [24] R. E. Nahory and J. L. Shay, *Phys. Rev. Lett.* **21**, 1569 (1968).
- [25] K. Tharmalingam, *Phys. Rev.* **130**, 2204 (1963).
- [26] D. Goldhaber-Gordon, J. Göres, M. A. Kastner, H. Shtrikman, D. Mahalu, and U. Meirav, *Phys. Rev. Lett.* **81**, 5225 (1998).
- [27] N. Tancogne-Dejean, M. A. Sentef, and A. Rubio, *Phys. Rev. B* **102**, 115106 (2020).
- [28] N. Maeshima and K. Yonemitsu, *J. Phys.: Conf. Ser.* **21**, 183 (2005).
- [29] J. D. Lee and J. Inoue, *Phys. Rev. B* **76**, 205121 (2007).
- [30] T. Kaneko, T. Shirakawa, S. Sorella, and S. Yunoki, *Phys. Rev. Lett.* **122**, 077002 (2019).

- [31] S. A. Sato, H. Hirori, Y. Sanari, Y. Kanemitsu, and A. Rubio, *Phys. Rev. B* **103**, L041408 (2021).
- [32] D. Góra and K. Rosciszewski, *J. Phys.: Condens. Matter* **8**, 8995 (1996).
- [33] F. Dong and J. Liu, *Phys. Rev. A* **106**, 063107 (2022).
- [34] A. Srivastava and J. Kono, Postconference Digest Quantum Electronics and Laser Science, 2003. QELS., Baltimore, MD, USA, 2003, pp. 2 pp.-, doi: [10.1109/QELS.2003.238340](https://doi.org/10.1109/QELS.2003.238340).
- [35] See Supplemental Material at <http://link.aps.org/supplemental/10.1103/PhysRevB.108.035122> for more details.
- [36] M. B. J. Meinders, H. Eskes, and G. A. Sawatzky, *Phys. Rev. B* **48**, 3916 (1993).
- [37] Y. Kim and J. D. Lee, *npj Comp. Mater.* **6**, 132 (2020).
- [38] R. Jördens, N. Strohmaier, K. Günter, H. Moritz, and T. Esslinger, *Nature (London)* **455**, 204 (2008).
- [39] S. Wall, D. Brida, S. R. Clark, H. P. Ehrke, D. Jaksch, A. Ardavan, S. Bonora, H. Uemura, Y. Takahashi, T. Hasegawa, H. Okamoto, G. Cerullo, and A. Cavalleri, *Nat. Phys.* **7**, 114 (2011).
- [40] M. Mitrano, G. Cotugno, S. R. Clark, R. Singla, S. Kaiser, J. Stähler, R. Beyer, M. Dressel, L. Baldassarre, D. Nicoletti, A. Perucchi, T. Hasegawa, H. Okamoto, D. Jaksch, and A. Cavalleri, *Phys. Rev. Lett.* **112**, 117801 (2014).